Ontogeny of the anuran urostyle and the developmental context of evolutionary novelty

Gayani Senevirathne[a], Stephanie Baumgart[a], Nathaniel Shubin[b], James Hanken[c,d], and Neil H. Shubin[a,1]

[a]Department of Organismal Biology and Anatomy, University of Chicago, Chicago, IL 60637; [b]Laboratory Schools, University of Chicago, Chicago, IL 60637; [c]Department of Organismic and Evolutionary Biology, Harvard University, Cambridge, MA 02138; and [d]Museum of Comparative Zoology, Harvard University, Cambridge, MA 02138

Contributed by Neil H. Shubin, December 5, 2019 (sent for review October 8, 2019; reviewed by Marvalee H. Wake and John Wallingford)

Developmental novelties often underlie the evolutionary origins of key metazoan features. The anuran urostyle, which evolved nearly 200 MYA, is one such structure. It forms as the tail regresses during metamorphosis, when locomotion changes from an axial-driven mode in larvae to a limb-driven one in adult frogs. The urostyle comprises of a coccyx and a hypochord. The coccyx forms by fusion of caudal vertebrae and has evolved repeatedly across vertebrates. However, the contribution of an ossifying hypochord to the coccyx in anurans is unique among vertebrates and remains a developmental enigma. Here, we focus on the developmental changes that lead to the anuran urostyle, with an emphasis on understanding the ossifying hypochord. We find that the coccyx and hypochord have two different developmental histories: First, the development of the coccyx initiates before metamorphic climax whereas the ossifying hypochord undergoes rapid ossification and hypertrophy; second, thyroid hormone directly affects hypochord formation and appears to have a secondary effect on the coccygeal portion of the urostyle. The embryonic hypochord is known to play a significant role in the positioning of the dorsal aorta (DA), but the reason for hypochordal ossification remains obscure. Our results suggest that the ossifying hypochord plays a role in remodeling the DA in the newly forming adult body by partially occluding the DA in the tail. We propose that the ossifying hypochord-induced loss of the tail during metamorphosis has enabled the evolution of the unique anuran *bauplan*.

bone | cartilage | metamorphosis | tadpoles | neurons

Vertebrate diversification is punctuated by the origin of structural and developmental novelties (e.g., refs. 1–4). The pronounced key innovation that distinguishes all anurans (frogs and toads), and enabled them to occupy new niches, is the evolution of saltatory locomotion (jumping). This innovation entails remarkable structural and developmental changes, which compose the anuran *bauplan*.

The anuran *bauplan*, conserved across the clade and characteristic of all adults, includes several features: loss of a tail, a shortened vertebral column, long hind limbs, radical transformation of the sacral region, and ventral articulation of the posterolaterally oriented pelvic girdle with a rod—the urostyle—lying between the paired ilia. The developmental processes underlying the emergence of the urostyle have received surprisingly little attention.

The urostyle is first observed in the fossil record in the Early Jurassic and has remained a conserved feature for over 200 million y (5, 6). It plays a major role in transmitting thrust from the hind limbs to the axial column during limb-driven locomotion (5, 6). The urostyle articulates with the posterior end of the sacrum and is a composite structure, comprising an ossified hypochord ventrally and a coccyx dorsally (7, 8).

The developmental origin of the anuran urostyle has been a source of speculation for over a century. Griffiths (9) proposed that the urostyle originates as a posterior outgrowth of the first postsacral intervertebral body, but this claim was disputed later when it was observed that the hypochord forms ventral to the notochord (i.e., outside of the perichondral bone). Later, some authors suggested that the urostyle forms by the fusion of a variable number of caudal vertebrae, and some even stated that the urostyle originates from a single cartilaginous rod (e.g., refs. 10 and 11). However, these ideas waned with the discovery that the urostyle forms from two discrete units: coccyx and hypochord (7, 8, 12).

The coccyx has a mesodermal origin and is derived from sclerotomal (paraxial mesoderm) cells (7, 12, 13). The coccyx fuses with the ossified hypochord at the onset of metamorphosis. Forming independently from the vertebral column, an ossifying hypochord is only present in anurans. An embryonic hypochord (nonossified), however, is seen in fishes, amphibians, and lampreys (14–19), but absent in amniotes. It is a rod-like structure located ventral to the notochord. The source of the embryonic hypochord needs deeper scrutiny and is argued to be of endodermal origin [e.g., zebrafish (17) and amphibians (15, 16, 18, 20)] or derived from the superficial mesodermal layer [e.g., amphibians (21) and zebrafish (22, 23)]. Compared to the coccyx, the hypochord arises from an independent cell population that is not derived from the paraxial mesoderm (12). The embryonic hypochord, which is only present in anamniotes, secretes vascular endothelial growth factor (VEGF) and patterns nearby blood vessels (16, 18). Even though amniotes lack a hypochord, it

Significance

Fusion of caudal vertebrae has evolved multiple times independently: the pygostyle of birds, coccyx in apes and humans, ural plate of fish, and the urostyle of frogs. The anuran urostyle, however, is structurally and developmentally distinct because of the contribution of an ossifying hypochord. To date, the developmental mechanisms behind an ossifying hypochord have remained obscure. Here, we provide a detailed analysis of the development of this evolutionary innovative structure and of how neuromusculature, cell death, and proliferation paved their way to facilitate its formation. Finally, we propose that the ossifying hypochord plays a role in tail loss in anurans and reorganizing the dorsal aorta and thus is pivotal in the evolution of the anuran *bauplan*.

Author contributions: G.S., J.H., and N.H.S. designed research; G.S., S.B., and N.S. performed research; N.H.S. contributed new reagents/analytic tools; G.S., J.H., and N.H.S. analyzed data; and G.S., J.H., and N.H.S. wrote the paper.

Reviewers: M.H.W., University of California, Berkeley; and J.W., University of Texas at Austin.

The authors declare no competing interest.

Data deposition: Computed tomography (CT) scan data reported in this study are available on MorphoSource, under the project name "Ontogeny of the Urostyle" (accession no. P884; doi:10.17602/M2/M97424, doi:10.17602/M2/M97371, doi:10.17602/M2/M97372).

See online for related content such as Commentaries.

[1]To whom correspondence may be addressed. Email: nshubin@uchicago.edu.

This article contains supporting information online at https://www.pnas.org/lookup/suppl/doi:10.1073/pnas.1917506117/-/DCSupplemental.

First published January 27, 2020.

has been shown that the dorsal endoderm of amniotes has taken over the function of the hypochord where the dorsal endoderm forms close to blood vessels and secretes VEGF in a similar manner (24, 25).

In embryonic amphibians, the hypochord (nonossified) lies flat over the notochord once its function of positioning the dorsal aorta is completed (15, 16), but it is retained in the postsacral region only in anurans (12). Many questions still remain unanswered regarding the ossifying hypochord: How and why does this structure ossify only in anurans? What initiates its formation? What is the function of it?

Using an integrative approach, we show how the axial skeleton, cellular composition, neuromuscular system, spinal cord, and vasculature change during development of the urostyle, focusing on the ossifying hypochord. We discuss the novelty of this structure and compare it across the convergently evolved caudal fusions.

Results

Coccyx and Hypochord Develop during Metamorphic Climax. We stained cartilage and bone using Alcian blue and alizarin red, respectively. The majority of postcranial elements complete ossification before metamorphic climax (a detailed description of the axial column ossification is given in *SI Appendix*). Coccygeal formation is initiated during prometamorphosis (stage 54) when cartilaginous postsacral vertebra I (PSI) forms (*SI Appendix*, Fig. S1). PSI is triangular-shaped and narrower than other presacral vertebrae (Fig. 1 *A*–*C*). By stage 61, the neural pedicels of PSII are ossified, and PSII continues to extend in length anteroposteriorly. At this stage, hypochord ossification is also initiated ventral to the notochord, and PSII appears as a slender ossifying stripe (Fig. 1 *A*–*C*).

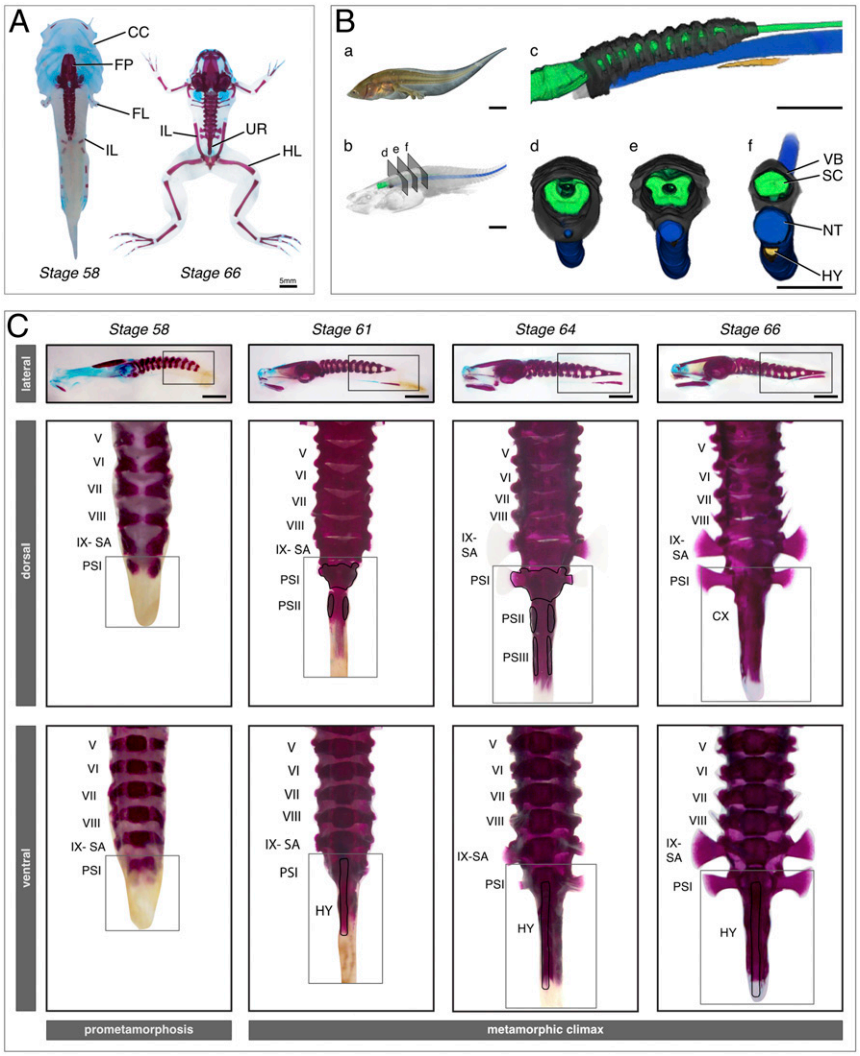

Fig. 1. Bone and cartilage formation of the urostyle. (*A*) Dramatic skeletal remodeling at metamorphic climax in *X. tropicalis* visualized through cartilage and bone staining, using Alcian blue and alizarin red, respectively. Cartilage is depicted in blue; bone is depicted in red. The larval chondrocranium remodels and forms new cranial bones. The urostyle forms during metamorphic climax and lies between the two ilia. (*B*) CT-scanned tadpole of *X. tropicalis*, NF stage 61 (metamorphic climax, day 2), highlighting axial skeleton formation at the rostral end of the tadpole body. The coccyx and the hypochord form midlength of the body, and the tail resorbs completely during metamorphosis. (*a*) Photograph of a live NF-61 tadpole; (*b*) CT-scanned tadpole after volume rendering; (*c*–*f*) Segmented tadpole highlighting the spinal cord, axial column, notochord, and hypochord. (*C*) Coccyx and hypochord formation at metamorphic climax in *X. tropicalis*. The coccyx is initiated as two ossification centers, which extend posteriorly and anteriorly. The hypochord forms ventral to the notochord and fuses with the coccyx at the end of metamorphic climax. Dorsal and ventral views are higher magnification images of the selected areas of the lateral view of each corresponding stage. The selected vertebrae are numbered from I to IX. CC, chondrocranium; CX, coccyx; FL, forelimb; FM, femur; FP, frontoparietal; HL, hind limb; HY, hypochord; IL, ilium; NT, notochord; PS, postsacral; SA, sacrum; SC, spinal cord; UR, urostyle; VB, vertebrae. (Scale bars: 5 mm.)

By stage 63, the hypochord has extended in length anteroposteriorly (Fig. 1*C*). The PSIII neural arches form by stage 64, and PSII and PSIII extend anteroposteriorly (Fig. 1*C*). Concomitantly, the hypochord extends anteriorly to the anterior-most margin of the sacrum and posteriorly to the posterior-most margin of PSIII. By stages 65 and 66, notochordal degeneration has initiated, and PSII and PSIII have fused, forming two strips of ossifications, losing the myomere boundaries. PSI fusion with the anterior margins of PSII happens subsequently (Fig. 1*C*). At the end of metamorphosis, the cone-shaped coccyx has fused synostotically with the hypochord.

Osteocyte–Chondrocyte Differentiation at the Sites of Urostyle Development. The cells contributing to the coccyx have a paraxial mesodermal origin (12), and the embryonic hypochord is argued to be derived from the endoderm/superficial mesoderm (15–25). However, not much is known about the ossifying hypochord. We conducted histology of sectioned tissues and focused on ossification patterns of the hypochord. The sclerotome in frogs is formed in both rostral and caudal somites (26), but only the rostral somites (somites 1 to 12 in *Xenopus tropicalis*) contribute to the axial column (12, 13); somites 9 to 12 contribute to the coccyx (equals fused postsacral vertebrae I to III) (8, 12). The bony coccyx forms from three ossification centers, which subsequently enlarge via endochondral ossification (a detailed description of coccyx formation is given in *SI Appendix*).

At the onset of metamorphosis, the ventral connective tissue around the notochord grows by increasing the number of cell layers (Fig. 2 *D*, *D″*, and *H* and *SI Appendix*, Figs. S3–S5). The undifferentiated cells giving rise to the ossifying hypochord (here referred to as osteo-chondro progenitors) aggregated and formed cartilaginous condensations (*SI Appendix*, Fig. S5), which were seen within the body region (*SI Appendix*, Figs. S3–S5) but not in the tail (*SI Appendix*, Figs. S3–S5). Hypertrophic chondrocytes were visible in the ventral portion of the hypochord; osteoblasts formed below the chondrocyte layer and began forming the perichondrium (Fig. 2 *D*, *D″*, and *H* and *SI Appendix*, Figs. S4 and S5). Within 2 d into metamorphic climax, hypertrophic chondrocytes differentiated and deposited cartilaginous extracellular matrix (ECM); the perichondrium with developing mineralized ECM was observed subsequently. Hypochordal ossification was more rapid relative to that of the coccyx (Fig. 2 *B*, *B″*, *D*, *D″*, *F*, and *F″*). Initial hypochordal chondrocytes accumulated along the midline of the tadpole body and formed a rod, with more cells accumulating on lateral sides of the hypochord (*SI Appendix*, Figs. S3–S5). Cells at the lateral-most margins of the hypochord are irregular in shape with numerous filopodia and appear to be migrating from the connective tissue around the notochord (*SI Appendix*, Fig. S6). Future studies are needed using a cell-tracing method to validate if it is the endoderm-derived embryonic hypochordal cells that undergo a cell-fate change during metamorphosis or if it is mesodermal cells that undergo ossification.

Thyroid Hormonal Control during the Formation of the Urostyle. Thyroid hormone (TH) peaks during metamorphic climax (27–31) and controls many structural modifications that a tadpole undergoes during metamorphosis, including loss or remodeling of larval cartilage and de novo formation of bones (32–34). To see if TH affects the formation of the urostyle, which also forms at metamorphic climax, we inhibited TH using methimazole in stage-54 tadpoles; methimazole inhibits thyroid gland function and prevents metamorphosis (35–37). The axial column is partially developed by stage 54 (*SI Appendix*, Fig. S1), making it an ideal stage to begin testing the effect of TH on urostyle formation. After 2 mo, the control tadpoles metamorphosed normally, but the methimazole-treated tadpoles had not completed metamorphosis and had halted their development (*SI Appendix*, Fig. S8). TH-inhibited tadpoles had incomplete development of the coccyx: the neural arches of PSI and PSII were developed (*SI Appendix*, Fig. S8), but PSI and PSII remained unfused. The coccygeal morphology of the methimazole-treated tadpoles resembled a stage-61 tadpole in the control experiment. However, hypochord formation was disrupted entirely (*SI Appendix*, Fig. S8). Partial coccygeal development and no hypochordal development (*SI Appendix*, Fig. S8) suggest the possibility of coccyx and hypochord being controlled by two developmental triggers. Hence, we hypothesize that the larval hypochordal cells (at myotome 8 to 12) undergo chondrogenesis and osteogenesis in the presence of TH and contribute to the ossifying hypochord during metamorphosis in anurans.

Muscular Remodeling near the Urostyle. A tadpole body possesses myotomes (dorsalis trunci [DT]) that undergo secondary myogenesis during metamorphosis (38–40). Three muscles are connected to the urostyle in an adult frog: longissimus dorsi (LD), coccygeo-iliacus (CI), and coccygeo-sacralis (CS) (6, 41). This muscle arrangement enables saltation in anurans (6). We conducted whole-mount and section-immunohistochemistry to observe the change in muscular composition with respect to the coccyx/hypochord formation, tail and notochord degeneration, and change in muscle fiber width. Before metamorphosis, the tadpole body (Fig. 3 *A*, *D*, and *D″*) and tail (*SI Appendix*, Fig. S9) possessed muscle fibers that were between 20 and 150 μm wide. With the onset of metamorphosis (stage 61) (*SI Appendix*, Fig. S10), the dorsal-most muscles (newly forming longissimus dorsi [LD]) increased in the number of muscle fibers and decreased in fiber diameter (<20 μm). LD was the first urostyle-associated muscle to form by stage 61 (*SI Appendix*, Fig. S10). Most of the ventral muscle margins disappeared (Fig. 2*E′*), and only the lateral and dorsal-most muscles were apparent (*SI Appendix*, Fig. S10). By stage 63, CI started to form (Fig. 3 *E* and *E″*). At the end of metamorphosis, LD had increased in area (Fig. 3 *F* and *F″* and *SI Appendix*, Fig. S11) and in the number of muscle fibers; the area of DT had decreased (*SI Appendix*, Figs. S11 and S13), and the number of muscle fibers had decreased (Fig. 3 *F* and *F″*). Ventrally, two muscles were evident: CS and CI (CI is the last muscle to form), which were attached to the developing urostyle (Fig. 3 *F* and *F″*). The number of muscle fibers of CS and CI was reduced, and muscle fiber width had increased (>100 μm) compared to the ventral larval muscles seen at prometamorphosis and at the beginning of metamorphic climax. A close look at the sarcomere proteins of the muscles near the urostyle before, during, and at the end of metamorphic climax indicates that the muscle sarcomeres are disorganized with the onset of metamorphosis (*SI Appendix*, Fig. S12). Our findings suggest that the muscles near the developing urostyle may be undergoing "myofiber turnover"—a phenomenon that can be recognized by the large, larval myofibers degenerating and small muscle fibers forming and replacing the larval ones (42–45). However, the change in myofiber width could also be due to reshaping of the myofibers, corroborant with the posterolateral rotation of the pelvic girdle (*SI Appendix*, Fig. S7). Future studies using a cell-lineage tracing method are needed to better understand these events.

Remodeling of the Spinal Cord and Peripheral Nervous System Adjacent to the Urostyle. The spinal cord and peripheral nervous system (PNS) differ between tadpoles and adults (46–48). To see how innervation and the spinal cord change at the sites of the future urostyle, we conducted whole-mount and section-immunohistochemistry. The spinal cord in transverse cross-sections across caudal myomeres XII to XIV appeared comparatively smaller than the presacral spinal cord (*SI Appendix*, Fig. S9), but larger than the tail spinal cord (*SI Appendix*, Fig. S9). At the end of metamorphosis, the spinal cord (referred to as the filum terminale in adults) is visible as fibrous tissue, and axons

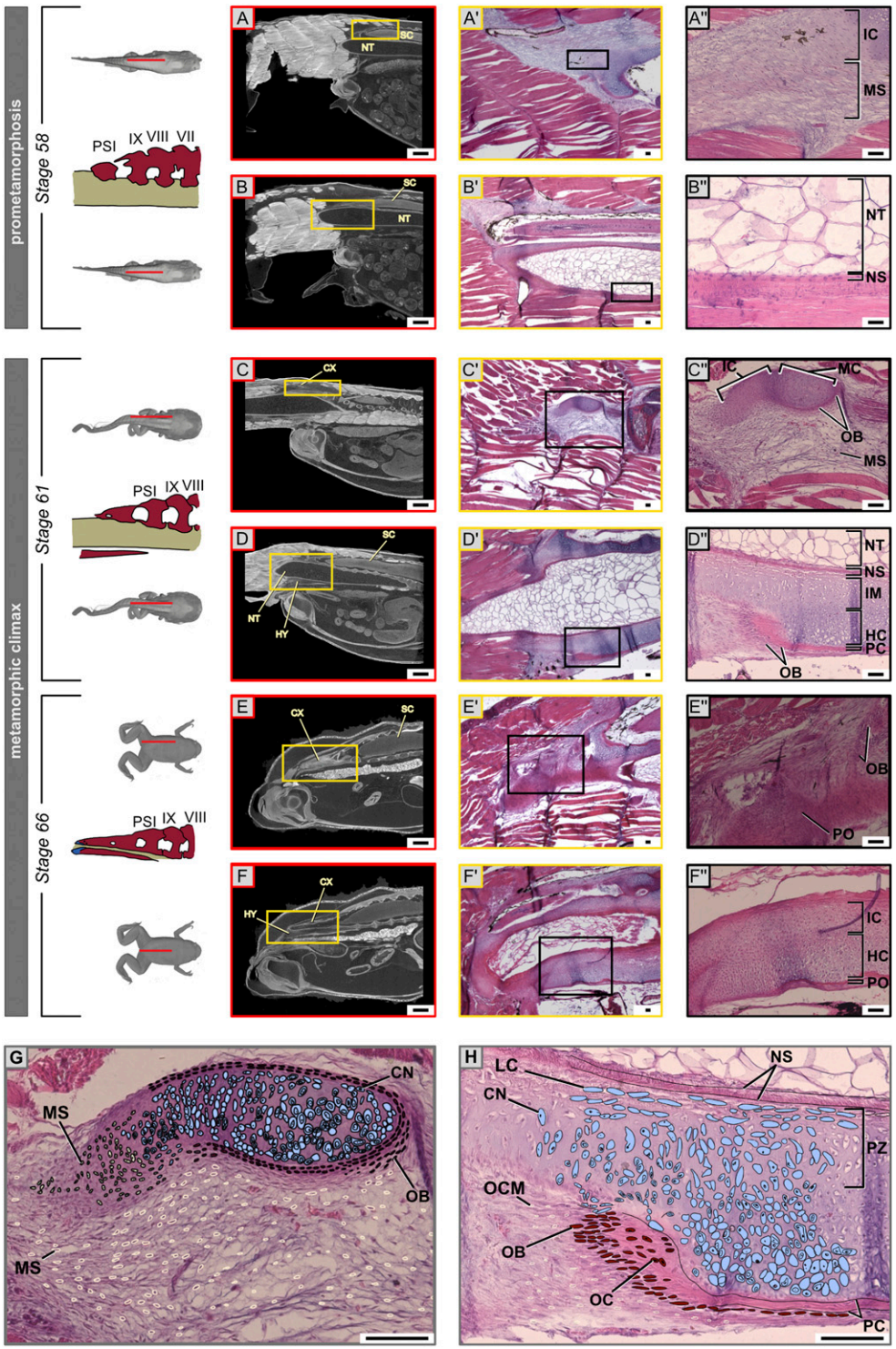

Fig. 2. Chondrocyte–osteocyte differentiation during urostyle formation. (*A*–*H*) Hematoxylin (stains nuclei purple) and eosin (stains cytoplasm and extracellular matrix pink) staining of histological sections (sagittal, *A*′–*F*′) and orthoslices (sagittal, *A*–*F*) of CT scans of *X. tropicalis* at the site of urostyle formation. The *Upper Row* of each stage corresponds to a left parasagittal section. The *Lower Row* of each stage depicts a midsagittal section. Magnified cells in the last column (*A*″–*F*″) are cells of interest, which change during development. (*A*′, *B*′, *A*″, and *B*″) At stage 59, undifferentiated mesenchymal cells (scleroblasts) at the sites of the future coccyx aggregate to form mesenchymal condensations that form the rudimentary neural arches; osteo-chondro progenitors of the hypochord are present ventral to the notochordal sheath. (*C*′, *D*′, *C*″, and *D*″) Cartilaginous condensations are visible as immature chondrocytes and mature chondrocytes. Chondrocytes in the ossifying coccyx and hypochord; the perichondrium starts to form around the mature chondrocytes. (*E*′, *F*′, *E*″, and *F*″) The periosteum forms with the degeneration of the cartilaginous matrix, but, during hypochord ossification, hypertrophic chondrocytes degenerate, and some dedifferentiate into osteocytes. (*G* and *H*) Illustrations of ossification patterns of the coccyx and hypochord, highlighting the proliferating zone, growth zone, and ossifying zones for the two tissue types. CN, chondrocytes; CX, coccyx; ECM, extracellular matrix; HC, hypertrophic chondrocytes; HY, hypochord; IC, immature chondrocytes; IM, immature cartilage cells; LC, lacunae; MC, mature chondrocytes; MS, mesenchymal cells (scleroblasts); NS, notochordal sheath; NT, notochord; OB, osteoblasts; OC, osteocytes; OCM, osteo-chondro progenitors; PC, perichondrium; PO, periosteum; PZ, proliferating zone; SC, spinal cord. (Scale bars: 2 mm (*A*–*F*) and 100 μm.)

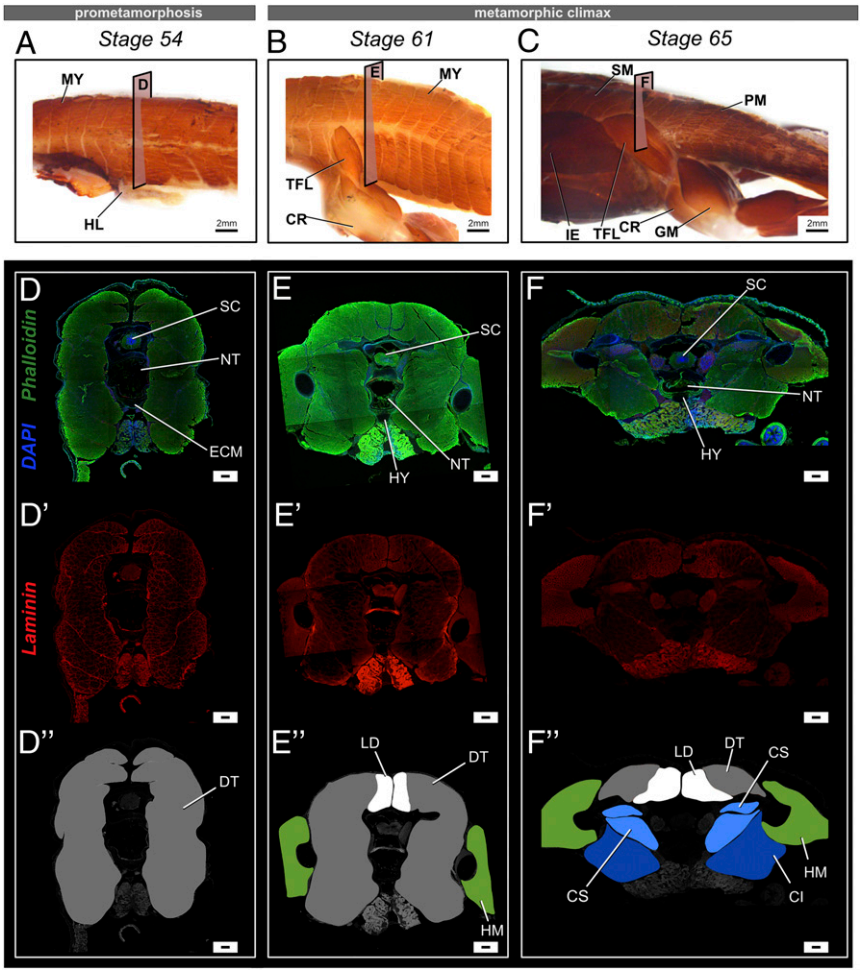

Fig. 3. Changes in muscle composition near the urostyle before and after metamorphosis in *X. tropicalis*. (*A*–*C*) Lateral views of whole-mount immunostained specimens for skeletal muscle marker 12-101 at stages 54 (*A*), 61 (*B*), and 65 (*C*). Before metamorphic climax, primary muscles are undifferentiated and referred to as dorsal trunci (DT). During metamorphic climax, the myomeres undergo secondary myogenesis and form new muscle types, which differ in muscle fiber width and are attached to the newly forming skeletal structures. The coccygeo-iliacus originates from the lateral surface of the urostyle; the longissimus dorsi originates from the dorsal part of the urostyle and extends anteriorly; and the coccygeo-sacralis connects the sacrum and the coccyx. (*D*–*F* and *D′*–*F′*) Transverse cross-sections across the trunk myotome XII at prometamorphic and metamorphic stages, where phalloidin (green) stains the extracellular matrix, DAPI (blue) stains nuclei, and laminin (red) stains muscle fibers. (*D*, *D′*, and *D″*) Comparison of muscle fiber width shows that primary muscles have a constant width across the trunk body. (*E′* and *F′*) Newly differentiating muscles (dorsal-most muscles) are smaller in fiber width. (*D″*–*F″*) Illustrations of the transverse cross-sections of the respective stages highlighting the different types of primary and secondary muscles. CI, coccygeo-iliacus; CR, cruralis; CS, coccygeo-sacralis; DT, dorsalis trunci; GM, gluteus magnus; HL, hind limb; HM, hind limb muscles; IE, iliacus externus; LD, longissimus dorsi; MY, myomeres; PM, primary muscles; SM, secondary muscles; TFL, tensor fasciae latae. (Scale bars: 2 mm (*A*–*C*) and 100 μm.)

project outwards from the spinal foramina (Fig. 4 and *SI Appendix*, Fig. S9). The filum terminale had myelinated fibers running anteroposteriorly (Fig. 4 *F* and *F′* and *SI Appendix*, Fig. S9). When the tail started to degenerate, the spinal nerves at the posterior-most end of the tail also degenerated (Fig. 4*C* and *SI Appendix*, Fig. S11). Spinal nerve X exited through the spinal nerve foramina of the urostyle, and the rest of the caudal spinal nerves degenerated concordant with the fusion of the coccyx and hypochord (Fig. 4*C*).

Dorsal Aorta and the Ossifying Hypochord. The embryonic hypochord (nonossified) forms after 3 to 4 d in a developing embryo and helps position the dorsal aorta (DA) (15). After the DA is formed, the hypochord degenerates completely in fishes and salamanders (15, 16), but it ossifies at the midlength of the tadpole body in anurans and contributes to the axial column (12). To see if the ossifying hypochord plays a role in major blood vessel reorganization during metamorphosis, we reconstructed the DA, posterior cardinal vein (PCV), and dorsolateral anastomosing vessel (DAV) in metamorphosing tadpoles using micro-computed tomography (microCT) scans (*SI Appendix*, Figs. S14 and S15). The DA was present ventral to the notochord along the trunk, the PCV was ventral to the DA before metamorphosis (Fig. 5 *A*, *A′*, and *C* and *SI Appendix*, Figs. S3 and S12), and the DAV was dorsal to the spinal cord; the DAV and PCV merged ventral to the PSI (myomere XI). At the onset of metamorphosis, the hypochord ossified dorsal to the DA (Fig. 5*C* and *SI Appendix*, Fig. S14). By stage 63, when the hypochord reached its maximum length, the DA was occluded at the posterior-most end of the hypochord (Fig. 5*C* and *SI Appendix*, Fig. S14). This occlusion could be a reason for the accelerated tail resorption within the next 2 to 3 d during metamorphic climax (Fig. 5 *B*, *B′*, and *C*). Tail resorption is evident by the sudden pigmentation change (Fig. 5 *B* and *B′*) and is likely due to blood loss in the tail (49). After partial occlusion of the DA, it was remodeled into two branches that form iliac arteries and enter the hind limbs (Fig. 5 *B*, *B′*, and *C* and *SI Appendix*, Fig. S15).

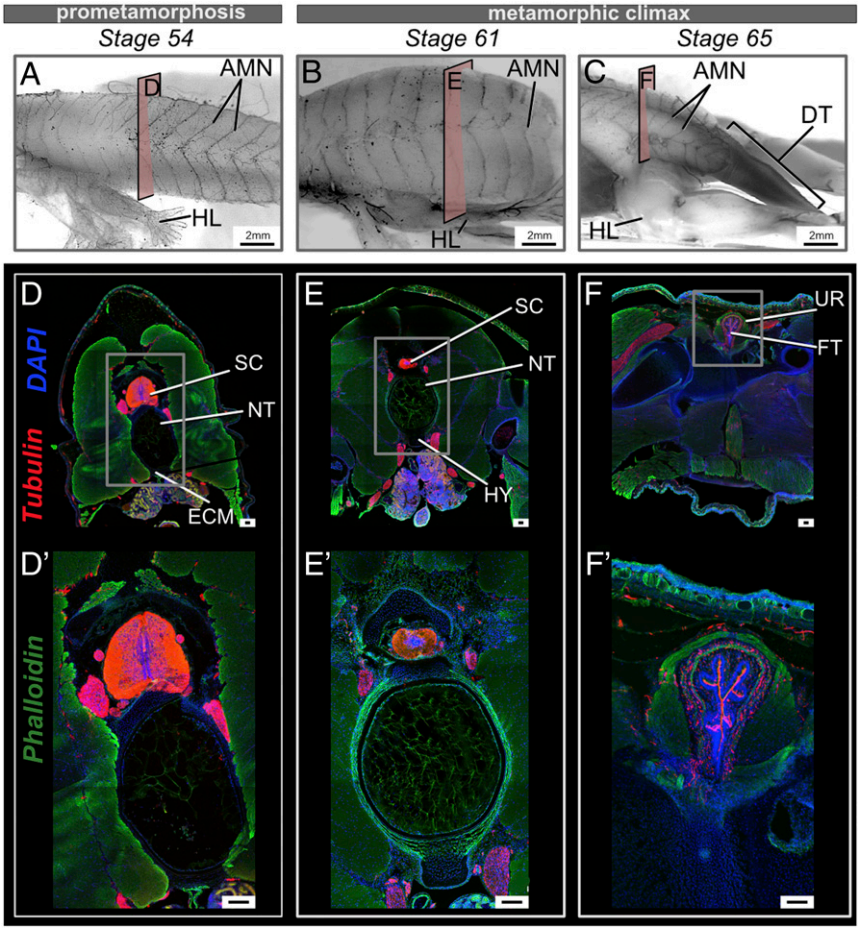

Fig. 4. Changes in the spinal cord and innervation at the sites of urostyle formation during development. (*A*–*C*) Lateral views of whole-mount immunostained tadpoles using acetylated tubulin, at stages 54 (*A*), 61 (*B*), and 66 (*C*). Before tail regression is initiated, the axial myomeres possess axial motor neurons (AMNs), equally distributed, but AMNs degenerate with the regressing tail during metamorphic climax. (*D*–*F*) Transverse cross-sections across trunk myotome XII at prometamorphic and metamorphic stages, immunostained for acetylated tubulin (red), extracellular matrix (green), and nuclei (blue). (*D′*–*F′*) Magnified images of the spinal cord for each corresponding stage. (*D*, *D′*, *E*, and *E′*) The spinal cord is recognizable as gray matter (in the middle) and white matter (surrounding the gray matter) in transverse cross-sections. (*F* and *F′*) The spinal cord changes shape with the fusion of the coccyx and hypochord and is referred to as the filum terminale. AMN, axial motor neurons; DT, degenerating tail; ECM, extracellular matrix; FT, filum terminale; HL, hind limb; HY, hypochord; NT, notochord; SC, spinal cord; UR, urostyle. (Scale bars: 2 mm (*A*–*F*) and 100 μm.)

Cell Death and Cell Proliferation. Cell death and cell proliferation are two key processes of metamorphic climax (34). To assess how these two phenomena affect bones, cartilage, neurons, and muscles at the site of the urostyle, we conducted cell proliferation (using anti–5-bromo-2-deoxyuridine [BrdU]) and cell death (anti-caspase3 antibodies) immunohistochemistry on whole mounts and sections. Before metamorphosis (e.g., stage 58), cells proliferate near the dorsal-most muscles (Fig. 6 *A* and *A′* and *SI Appendix*, Fig. S16); no cell death was observed (Fig. 6 *D* and *D′*, stage 57). With the onset of metamorphic climax, dorsal-most and lateral muscles continued to divide (Fig. 6*B′*); innermost muscles surrounding the notochord and ventral-most muscles underwent apoptosis (Fig. 6*E′*). The lateral-most margin of the hypochord demarcated the proliferating chondrocyte zone (Fig. 6 *C*, *C′*, and *C″*) with increased cell proliferation; no cell death by apoptosis was observed at the sites with mature hypertrophic chondrocytes (Fig. 6 *G*, *G′*, and *G″*). Usually, mature hypertrophic chondrocytes (HCs) in an ossifying tissue undergo apoptosis (50–52). However, the HCs within the hypochord survived, even when the hypochord was mineralized and vascularized at the end of metamorphosis. These results suggest that there is a possibility that the terminal chondrocytes dedifferentiate into osteocytes. Such dedifferentiation is a phenomenon commonly seen in rapidly ossifying bones (53–56). By stage 63, dorsal-most and lateral muscles underwent apoptosis (Fig. 6 *F* and *F′*). Once the hypochord ossification reaches its maximum length (by stage 63), the tail length reduction is initiated and can be observed by the presence of phagocytotic cells within the tail region (Fig. 6 *H*, *H′*, *I*, and *I′*). With the fusion of coccyx and hypochord, the spinal cord also showed positive signal for cell apoptotic markers (Fig. 6 *G′* and *G″*), indicating the spinal cord only degenerates at the urostyle region.

Discussion

The anuran urostyle is a unique component of the vertebrate axial skeleton because it is formed from an ossifying hypochord, which contributes and fuses to the coccyx at the end of metamorphosis. In fishes, posterior-most centra fuse to form the ural, which supports the developing caudal fin (57–59). Within the actinopterygian lineage, recently evolved teleosts have experienced a reduction in caudal elements with the evolution of homocercal tails (compared to the plesiomorphic state of having heterocercal tails) (60–62). It has been hypothesized that having polyurals (more than two ural elements) is more primitive compared to the diural condition (60); all individuals go through some fusion of the urals after they are formed as individual

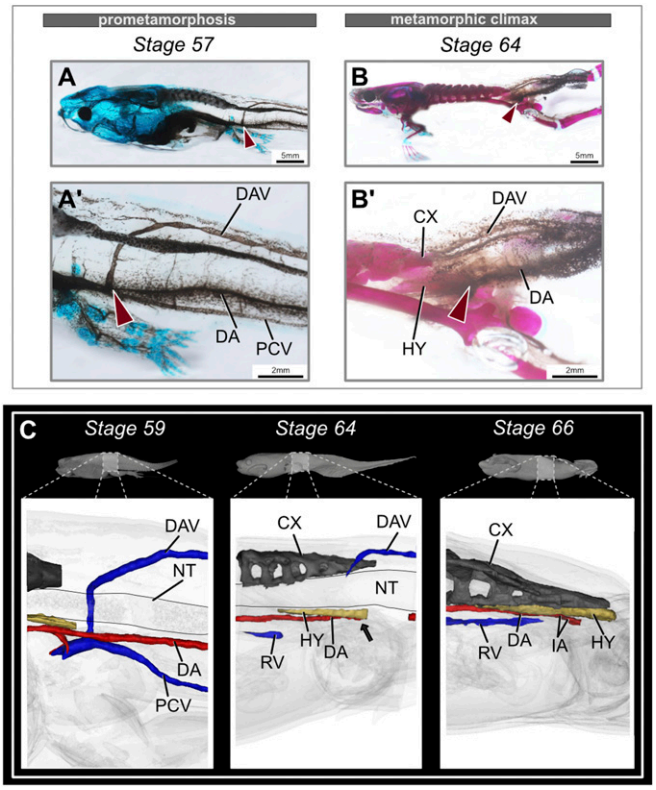

Fig. 5. Rearrangement of the major blood vessels during metamorphosis. (*A* and *B*) Comparison of the dorsal aorta and posterior veins in the tadpole tail during metamorphosis, lateral view. Before metamorphosis, the DA and PCV are present ventral to the notochord, and the DAV is present dorsal to the spinal cord. The DAV then merges with the PCV. At the end of metamorphosis, stage-64 tadpoles lose the DA partially, along with PCV and DA. Red arrows point at the merging of DAV and PCV. (*A′* and *B′*) Magnified images of the corresponding stage, highlighting the major blood vessels. (*C*) MicroCT-scanned tadpoles at prometamorphic and metamorphic climax stages. The black arrow points to the occlusion point of the DA at stage 64 (before the tail starts to regress). Stage 66 highlights the formation of new veins and rearrangement of the DA in the metamorphosed frog (refer to Datasets S1–S3 to observe this closely). CX, coccyx; DA, dorsal aorta; DAV, dorsolateral anastomosing vessel; HY, hypochord; IA, iliac artery; NT, notochord; PCV, posterior cardinal vein; RV, renal vein.

centra, and fish ural fusion progresses as a slow process (60, 63). Avian tails have also undergone considerable changes, from the plesiomorphic long tails of nonavian dinosaurs to the short tails with a fused pygostyle of birds (the group Pygostylia; this includes modern birds) as an adaptation for flight (64–66). During the embryonic period, pygostyle vertebrae chondrify, mineralize, and then fuse once the bird hatches (66). Tail loss has also evolved convergently in mammals, including apes and humans. This loss has resulted in the evolution of the coccyx, commonly known as the tailbone. The coccyx is formed by fusion of three to five coccygeal vertebrae (67–69), which fuse completely with no visible sutures or partially with sutures still visible, and it attaches to the sacrum.

Coccyx vs. Hypochord. We found that coccyx and hypochord show two different developmental patterns. Firstly, the coccyx ossifies in a segmental and comparatively slow manner whereas the hypochord ossifies as a single rod relatively quickly. Secondly, initiation of hypochordal ossification appears to be mediated by thyroid hormone whereas the coccyx is not; however, the postsacral vertebrae fusion was disrupted in methimazole-treated tadpoles (*SI Appendix*, Fig. S8). Further studies using early and late developmental stages of tadpoles and comparative transcriptomics of the two tissue types are required to validate TH control of urostyle formation.

Previous studies have shown that removal of the embryonic spinal cord or notochord disrupts the morphology and regionalization of the vertebral column (55, 70, 71). For example, removal of the notochord from *Ambystoma mexicanum* embryos resulted in a fused cartilaginous rod (70). Even though cartilage was developed, the differentiation or regionalization was disrupted. Even in mice, removing the neural tube results in abnormally segmented ossifications around the notochord, and notochord removal results in unsegmented cartilaginous sheaths (55, 71, 72). Studies have postulated that the notochord alone acts on the segmentation and notochord and spinal cord together influence the differentiation (71–76). We hypothesize that the switch that happens within the notochord during metamorphic climax (34) to secrete proteolytic enzymes may have disrupted its inductive abilities and that this could be a reason why regionalization at the urostyle site is disrupted or has been lost.

Ossifying Hypochord and the Anuran *Bauplan*. Why does the hypochord ossify only in anurans? The tail, contributing to more than half of the tadpole's length, is composed of muscles, neurons, blood vessels, and a notochord, and, hence, losing the tail rapidly is a developmental conundrum. It is suggested that the most vulnerable stage in terms of predation for a tadpole is when both its tail and four legs are present—the period leading up to metamorphic climax (77, 78). Hence, a developing tadpole needs to lose its tail efficiently and quickly to assume its adult body form. Therefore, the tail resorption process is completed within 2 to 3 d (79)—a remarkable evolutionarily favored transformation.

Tail loss has gained much attention over the past century mainly because of its importance in understanding the water-to-land transition. Previous work shows how increased TH at the beginning of metamorphic climax promotes autolysis of tail cells ("suicide model") (72, 73) (Fig. 6 *D′*, *E′*, and *F′*). However, the tail-length reduction, a result of cell phagocytosis ("murder model") (79, 80) (Fig. 6 *H*, *H′*, *I*, and *I′*), initiates only after 3 d into metamorphic climax and is not directly controlled by TH. The trigger of the "murder model" was overlooked in previous studies.

We propose that rapid tail loss in anuran larvae is related to ossification of the hypochord in the midlength of the body. Our results show how ossification of the hypochord may promote tail loss by remodeling the dorsal aorta (DA): DA occlusion occurs ventral to the posterior-most part of the hypochord (Fig. 5 and *SI Appendix*); subsequently, with the occlusion, the DA branches into two vessels ventral to the anterior-most margin of the hypochord, which enter the left and right hind limbs (Fig. 5 and *SI Appendix*, Figs. S14 and S15). This occlusion happens before the initiation of tail regression and posterolateral rotation of the pelvic girdle (Fig. 5 and *SI Appendix*, Figs. S7, S14, and S15). We propose that the low-pH environment resulting from the DA occlusion could be triggering the "murder model" in tadpoles.

The fossil record of anurans contains taxa having a tail with a few caudal vertebrae, which is the plesiomorphic state [e.g., Triassic *Triadobatrachus massinoti* (81) and *Czatkobatrachus polonicus* (82)], followed by the sudden appearance of forms with a urostyle and no tail (*Prosalirus bitis*) (5, 6). However, intermediate fossils between these two states have not been discovered. Our study points toward an explanation for the evolution of tail loss in anurans and the development of the urostyle: During the evolution of an anuran *bauplan*, hypochord ossification likely preceded loss of tail in salientians. Future studies creating genetic knockouts in anurans, either by preventing the ossification of the hypochord or by generating tailless tadpoles, would help us better understand the significance of the ossified hypochord and tail resorption during metamorphosis, while reiterating the novelty of the urostyle.

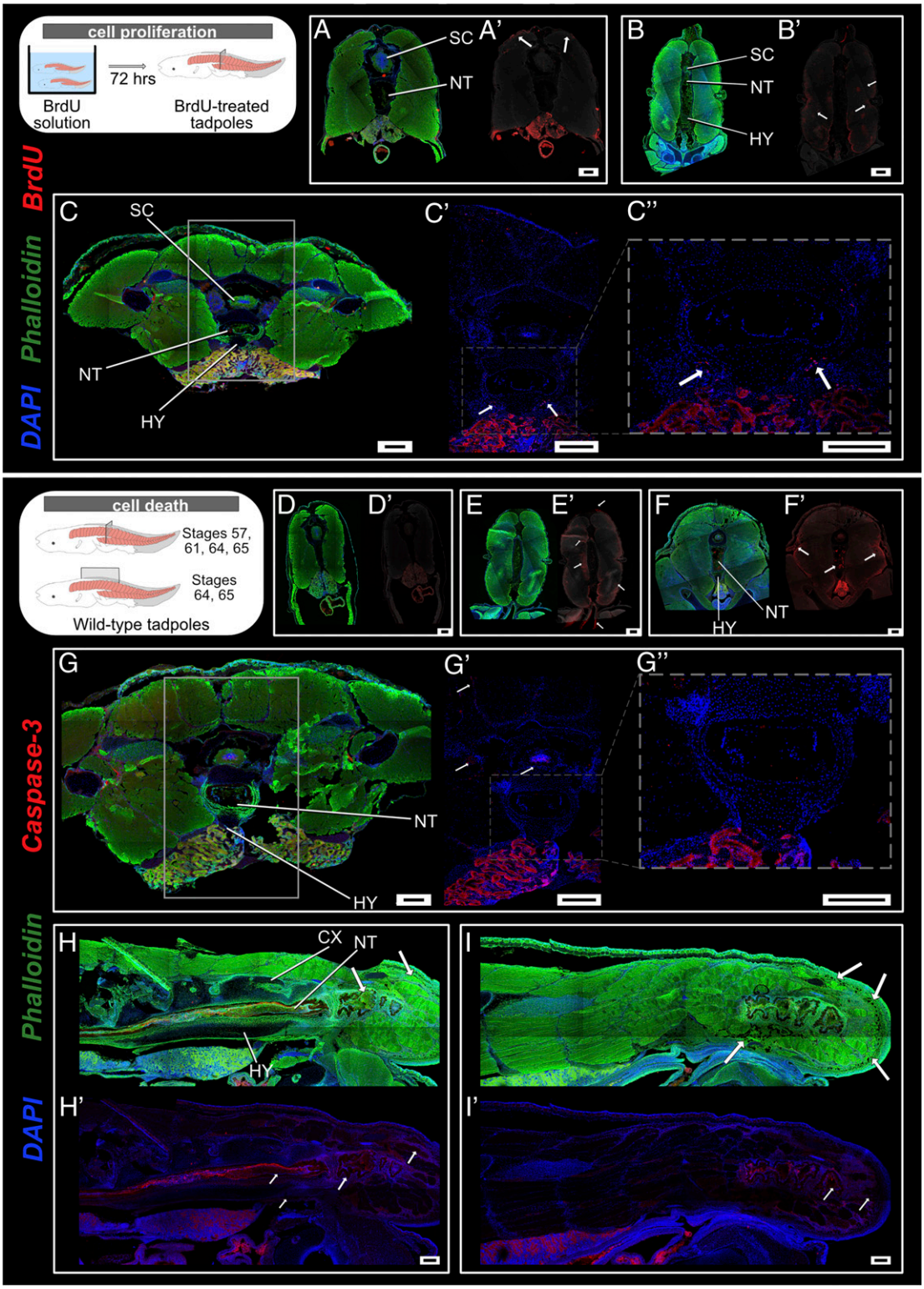

Fig. 6. Cell death and cell proliferation at the site of urostyle formation. (*A*–*C*) Transverse sections across trunk myotome XII, immunostained for anti-BrdU (red) to observe cell proliferation at stages 58 (*A* and *A*′), 61 (*B* and *B*′), and 64 (*C* and *C*′). (*A*′–*C*′) Anti-BrdU signal has been overlaid on a grayscale background to highlight the proliferating cells. Muscle cells initiate proliferation prior to metamorphic climax, starting with the dorsal-most muscles (*A*′). With the initiation of metamorphosis, muscles along the lateral margins proliferate (*B*′). Lateral margins of the hypochordal rod demarcate the chondrocyte proliferating zone (*C*, *C*′, and *C*″). White arrows depict proliferating zones. (*D*–*I*) Transverse and sagittal cross-sections across the trunk myotomes, immunostained for anti-Caspase 3 (red) to observe cell apoptosis. There is no cell death at stage 57, before metamorphic climax (*D* and *D*′). With the initiation of metamorphic climax at stage 61 (*E* and *E*′), innermost muscles surrounding the notochord and ventral-most muscles undergo apoptosis ("suicide model"). Dorsal-most and lateral larval muscle fibers undergo cell death at stage 63 (*F* and *F*′). By stage 64, the coccyx and hypochord have reached the maximum length by extending up to the myotome, and the spinal cord is degenerated (*G*, *G*′, and *G*″). Sagittal sections at stages 64 (*H* and *H*′) and 65 (*I* and *I*′) depict how the muscle cells are degenerated by phagocytosis ("murder model") with the reduction of the tail. CX, coccyx; HY, hypochord; NT, notochord; SC, spinal cord. (Scale bars: 100 μm.)

Materials and Methods

Different stages of *X. tropicalis* tadpoles were purchased from the National *Xenopus* Resource (NXR) at the Marine Biological Laboratory (MBL) (Woods Hole, MA). A nearly complete developmental series was obtained and euthanized using 0.2% aqueous tricaine methanesulfonate (MS-222), and the specimens were fixed in different fixatives according to each experiment. Tadpoles were staged according to Nieuwkoop and Faber (NF; 83). Developmental stages were obtained posthatching until the end of metamorphic climax. Refer to *SI Appendix*, Table S1 for the respective stages of the tadpoles, their total length (TL), and the number of replicates used in each experiment. All experiments were approved by the Marine Biological Laboratory (Protocol 18-42) and the University of Chicago (Protocol 72615).

Staining for Cartilage and Bone. The tadpoles were cleared and stained for bone and cartilage following Hanken and Wassersug (84) and Klymkowsky and Hanken (85). Euthanized stages were fixed in 4% neutral-buffered formalin from overnight to 4 d (depending on the size of the tadpoles) and subsequently stored in 70% ethanol until they were processed for staining. Developmental stages were dehydrated in absolute ethanol and stained for cartilage using Alcian blue. Following cartilage staining, specimens were rehydrated in a graded ethanol series (95%, 80%, 75%, 50%, 25%) and, finally, distilled water. Next, the muscles were digested in an enzyme solution (trypsin dissolved in 30% aqueous sodium borate). Subsequently, the bones were stained in alizarin red and destained in a solution of 1% KOH and 1% H_2O_2. The stained specimens were stored in glycerin and scored for bones/cartilage within 2 to 3 d of staining. Terminology for the bones, cartilage, and neuromuscular system follows Pugener and Magalia (8), Trueb (86), Duellman and Trueb (41), and Trueb and Hanken (87).

Histology. Euthanized stages were fixed in Bouin fixative (picric acid plus formaldehyde plus acetic acid) for between 24 h and 1 wk. The specimens were decalcified using a decalcifying solution (0.5 M EDTA, pH 7.0) for 30 min, washed in 1× phosphate-buffered saline (PBS) three times (20 min each), dehydrated in ethanol, and followed by three xylene washes. Subsequent paraffin washes were conducted at 70 °C, and, finally, tissues of interest were embedded in paraffin/paraplast molds. Paraffin-embedded specimens were sectioned at 10 μm using a rotatory microtome and mounted onto Fisherbrand Suprafrost microscope slides. Both sagittal and transverse sections were left overnight on a slide-heater at 35 °C. The sections were stained as follows: Initially, deparaffinization was done in two xylene washes, sections were rehydrated using an ethanol series and stained with Mayer hematoxylin (2 min) to visualize nuclei, and the slides were kept under running water for 20 min. Next, eosin stain was used to visualize cytoplasm and extracellular matrix. Subsequently, dehydration was done in an ethanol series and, finally, in xylene. The slides were mounted in xylene-based DPX, sealed with a coverslip (no. 1 thickness), observed under a Zeiss Axio Imager 2 microscope, and photographed using a Leica DFC 490 camera.

Thyroid Hormone and the Urostyle Development. Two experiments were conducted to visualize thyroid hormone (TH) involvement in urostyle development. Five stage-54 tadpoles were reared in 1 mM goitrogen methimazole (MMI) (Sigma-Aldrich; 100 mg/L of aquarium water) (31, 79, 88), and another five stage-54 tadpoles as the control experiment in 0.1 Marc's modified Ringer's (MMR) (1× MMR: 100 mM NaCl, 2 mM KCl, 1 mM $MgSO_4$, 2 mM $CaCl_2$, 5 mM Hepes, pH 7.4). The tadpoles were reared for 2 mo and then stained for bone and cartilage (see above) to see the effect of TH on urostyle development. This experiment was repeated twice.

Phosphomolybdic Acid Staining and CT Scanning. Five tadpoles (NF stages 58, 59, 61, 64, and 66) were dehydrated in 100% methanol, taken through a sucrose series, and left in 25% sucrose overnight or until the tadpoles sunk to the bottom. Finally, tadpoles were stained with 5% phosphomolybdic acid (PMA) dissolved in distilled water for 5 to 7 d. Tadpoles were washed in distilled water prior to scanning to get rid of excess stain. The specimens were scanned with the UChicago PaleoCT scanner (GE Phoenix v/tome/x 240kv/180kv scanner). The settings for close scans of the urostyle area were as follows: at 70 kV, 220 μA, no filtration, 3× averaging, exposure time of 1,000 ms per image, and a resolution of 6.3330 μm per slice (512 μm^3 per voxel). Whole bodies of tadpoles were scanned by using the following parameters: at 90 kVp, 190 μA, no filtration, 3× averaging, exposure time of 200 ms per image, and a resolution of 17.9820 μm per slice (512 μm^3 per voxel). Scanned images were analyzed and segmented using Amira 3D Software 6.0 (FEI) (Fig. 1*B*) and Materialize Mimics 22.0 segmentation software (Fig. 5*C*).

Cell Proliferation. Two tadpoles each from NF stages 55, 57, 61, and 63 were exposed to water containing 5-bromo-2-deoxyuridine (BrdU) (Sigma-Aldrich), 1 mg/mL, for 72 h to label the proliferating cells. The tadpoles were subsequently euthanized in MS-222 and fixed overnight in 4% paraformaldehyde (PFA) at 4 °C. The next day, the specimens were washed three times in ice-cold 1× PBS (15 min each) and transferred to 15% and 30% sucrose solutions. They were left overnight at 4 °C until they sank to the bottom of the tube. The tadpoles were then placed in Tissue-Tek O.C.T compound, flash frozen using liquid nitrogen, and sectioned at 20 to 25 μM using the Leica cryostat CM1900 and mounted on Fisherbrand SuperFrost Plus slides. Cryosections were rinsed three times in 1× PBS, permeabilized using 0.01% Triton/PBS solution, blocked in 2% skim milk solution, and incubated with the anti-BrdU (Sigma-Aldrich, mouse monoclonal; 2:1,000 concentration) for 1 h. The next day, the sections were washed three times in 0.25% Tween/PBS solution (10 min each), incubated in a solution of the secondary antibody (ThermoFisher, goat anti-mouse, Alexa Fluor 594, 2:1,000), phalloidin-Alexa 488 (Invitrogen, 1:1,000), and DAPI (Life technologies, 1:1,000) for 1 h. Finally, the cryosections were washed in 0.25% Tween/PBS solution, mounted in 50% glycerol, and visualized using a Zeiss 710 confocal microscope. The results were analyzed using Fiji image analysis software.

Section-Immunohistochemistry for Cell Death, Neurons, and Muscle Remodeling. Six tadpoles from each stage (stages 57, 60, 64, and 66) were fixed overnight in 4% PFA and frozen in Tissue-Tek O.C.T. using liquid nitrogen. The frozen samples were sectioned using a cryostat at 30 μM and were dried at room temperature for 30 min. Antibody staining was done as described in the preceding section: Tissues were permeabilized in Triton/PBS, blocked in 2% skim milk solution, and incubated overnight in the primary antibody solution. To observe cell death by apoptosis, anti–Caspase-3 antibody (Abcam ab13847, 2:1,000) was used; for neurons, acetylated Tubulin (Sigma, mouse monoclonal, 2:1,000) was used; for muscle fibers, Laminin antibody from the Developmental Studies Hybridoma Bank (DSHB) (3H11, 4:100) and anti-MyHC from DSHB (MF20, 1:20) were used; for sarcomere proteins anti-titin, anti-myomesin, and anti-tropomyosin were used (*SI Appendix*, Table S1). The next day, the tissues were washed in 0.25% Tween/PBS solution and incubated in the secondary antibody (mouse monoclonal, 2:1,000) plus Phalloidin (to visualize the extracellular matrix, 1:1,000) plus DAPI (nuclei, 1:1,000). Finally, the slides were washed in 0.25% Tween/PBS and visualized under a Zeiss 710 confocal microscope. The results were analyzed using the Fiji image analysis software.

Whole-Mount In Situ Hybridization and Whole-Mount Immunohistochemistry. Whole-mount in situ hybridization (WMISH) for the sclerotome marker *Pax9* was done as previously described (89). The primer sequences for the gene *Pax9* are as follows: forward, AGT AGG AAC ACG TTT CAG TCG; and reverse, TTG GAT CCT AGA GAT GAC AGC. After the color developed, the tadpoles were fixed overnight in 4% PFA at 4 °C, transferred to 30% sucrose solution, and flash frozen in OCT using liquid nitrogen. The tissues were sectioned using a Leica cryostat and mounted using 50% glycerol. The slides were photographed using a Leica DFC 490 camera. For whole-mount immunohistochemistry (WMIHC), tadpoles at stages NF 58, 59, 61, 63, and 66 were euthanized in MS-222 and fixed overnight in Dent fixative (methanol:dimethyl sulfoxide [DMSO] = 4:1) at room temperature. The staining was done as previously described (85, 90) with slight modifications. Tadpoles were washed in 1% PBTriton (1× PBS plus 1% Triton) for 3 h and transferred to 25% trypsin in PBS for 10 min. Next, they were transferred to precooled acetone for 20 min. Specimens were washed in 1% PBTriton and blocked overnight at 4 °C in a solution containing 1% PBTriton plus 10% goat serum plus 5% H_2O_2 plus 1% DMSO). Blocking solution was replaced by the primary antibodies: for muscles 12-101 (from DSHB, 1:50) and nerves (acetylated tubulin: Sigma, 1:1,000) and were left at 4 °C for 3 d. The tadpoles were washed five times in 1% PBTriton (1 h each) and transferred to the peroxidase-conjugated secondary antibody solution (The Jackson Laboratory 115-035-003, 1:1,000) in 10% goat serum plus 1% PBTriton. Finally, the specimens were washed in 1% PBTriton for 5 h and subjected to DAB reaction.

Data Deposition. The CT scanned data of stages 59, 64, and 66 have been submitted to MorphoSource with the DOIs 10.17602/M2/M97424, 10.17602/M2/M97371, and 10.17602/M2/M97372, under the project name "Ontogeny of the Urostyle" (accession no. P884) (91).

ACKNOWLEDGMENTS. We thank Marko Horb, Nikko-Ideen Shaidaini, and Marcin Wlizla (National Xenopus Resource [NXR], Marine Biological Laboratory) for husbandry and providing *X. tropicalis* tadpoles; Madhava Meegaskumbura for his comments on an early version of the manuscript; and Tetsuya Nakamura, Victoria Prince, and members of the N.H.S. laboratory for helpful discussions. This work was supported by University of Chicago Biological Sciences and the Brinson Foundation (N.H.S.); and by University of Chicago core facility funding (to G.S.).

1. S. M. Shimeld, P. W. H. Holland, Vertebrate innovations. *Proc. Natl. Acad. Sci. U.S.A.* **97**, 4449–4452 (2000).
2. D. H. Erwin, Novelty and innovation in the history of life. *Curr. Biol.* **25**, R930–R940 (2015).
3. A. C. Love, Explaining evolutionary innovation and novelty: Criteria of adequacy and multidisciplinary prerequisites. *Philos. Sci.* **75**, 874–886 (2008).
4. G. P. Wagner, V. J. Lynch, Evolutionary novelties. *Curr. Biol.* **20**, R48–R52 (2010).
5. N. H. Shubin, F. A. Jenkins, Jr, An early Jurassic jumping frog. *Nature* **377**, 49–52 (1995).
6. F. A. Jenkins, Jr, N. H. Shubin, *Prosalirus bitis* and the anuran caudopelvic mechanism. *J. Vertebr. Paleontol.* **18**, 495–510 (1998).
7. L. A. Pugener, "The vertebral column and spinal nerves of Anurans," PhD thesis, University of Kansas, Lawrence, KS (2002), p. 480.
8. L. A. Pugener, A. M. Maglia, Developmental evolution of the anuran sacro-urostylic complex. *South Am. J. Herpetol.* **4**, 193–210 (2009).
9. I. Griffiths, The phylogeny of the Salientia. *Biol. Rev. Camb. Philos. Soc.* **38**, 241–292 (1963).
10. H. F. Gadow, The evolution of the vertebral column: A contribution to the study of vertebral phylogeny. *J. Anat.*, 6–23 (1933).
11. A. S. Romer, The Chānares (Argentina) Triassic reptile fauna: VI. A chiniquodontid cynodont with an incipient squamosal-dentary jaw articulation. *Breviora* **344**, 1–18 (1970).
12. G. R. Handrigan, R. J. Wassersug, The anuran Bauplan: A review of the adaptive, developmental, and genetic underpinnings of frog and tadpole morphology. *Biol. Rev. Camb. Philos. Soc.* **82**, 1–25 (2007).
13. D. B. Wake, Aspects of vertebral evolution in the modern Amphibia. *Forma et Functio.* **3**, 33–60 (1970).
14. S. Hatta, On the formation of the germinal layers in *Petromyzon*. *J. Coll. Sci. Imp. Univ. Japan* **5**, 129–147 (1893).
15. J. Löfberg, A. Collazo, Hypochord, an enigmatic embryonic structure: Study of the axolotl embryo. *J. Morphol.* **232**, 57–66 (1997).
16. O. Cleaver, D. W. Seufert, P. A. Krieg, Endoderm patterning by the notochord: Development of the hypochord in *Xenopus*. *Development* **127**, 869–879 (2000).
17. J. Eriksson, J. Löfberg, Development of the hypochord and dorsal aorta in the zebrafish embryo (*Danio rerio*). *J. Morphol.* **244**, 167–176 (2000).
18. O. Cleaver, P. A. Krieg, VEGF mediates angioblast migration during development of the dorsal aorta in *Xenopus*. *Development* **125**, 3905–3914 (1998).
19. E. Lammert, O. Cleaver, D. Melton, Induction of pancreatic differentiation by signals from blood vessels. *Science* **294**, 564–567 (2001).
20. O. Cleaver, K. F. Tonissen, M. S. Saha, P. A. Krieg, Neovascularization of the *Xenopus* embryo. *Dev. Dyn.* **210**, 66–77 (1997).
21. D. R. Shook, C. Majer, R. Keller, Pattern and morphogenesis of presumptive superficial mesoderm in two closely related species, *Xenopus laevis* and *Xenopus tropicalis*. *Dev. Biol.* **270**, 163–185 (2004).
22. R. M. Warga, C. Nüsslein-Volhard, Origin and development of the zebrafish endoderm. *Development* **126**, 827–838 (1999).
23. A. E. Melby, R. M. Warga, C. B. Kimmel, Specification of cell fates at the dorsal margin of the zebrafish gastrula. *Development* **122**, 2225–2237 (1996).
24. D. J. Dumont *et al*., Vascularization of the mouse embryo: A study of flk-1, tek, tie, and vascular endothelial growth factor expression during development. *Dev. Dyn.* **203**, 80–92 (1995).
25. R. H. Row, S. R. Tsotras, H. Goto, B. L. Martin, The zebrafish tailbud contains two independent populations of midline progenitor cells that maintain long-term germ layer plasticity and differentiate in response to local signaling cues. *Development* **143**, 244–254 (2016).
26. R. S. Sánchez, S. S. Sánchez, Characterization of pax1, pax9, and uncx sclerotomal genes during *Xenopus laevis* embryogenesis. *Dev. Dyn.* **242**, 572–579 (2013).
27. D. D. Brown, L. Cai, Amphibian metamorphosis. *Dev. Biol.* **306**, 20–33 (2007).
28. S. Mukhi, L. Cai, D. D. Brown, Gene switching at *Xenopus laevis* metamorphosis. *Dev. Biol.* **338**, 117–126 (2010).
29. D. R. Buchholz, More similar than you think: Frog metamorphosis as a model of human perinatal endocrinology. *Dev. Biol.* **408**, 188–195 (2015).
30. D. R. Buchholz, *Xenopus* metamorphosis as a model to study thyroid hormone receptor function during vertebrate developmental transitions. *Mol. Cell. Endocrinol.* **459**, 64–70 (2017).
31. D. D. Brown, The role of deiodinases in amphibian metamorphosis. *Thyroid* **15**, 815–821 (2005).
32. J. Hanken, B. K. Hall, Skull development during anuran metamorphosis. II. Role of thyroid hormone in osteogenesis. *Anat. Embryol. (Berl.)* **178**, 219–227 (1988).
33. J. Hanken, C. H. Summers, Skull development during anuran metamorphosis: III. Role of thyroid hormone in chondrogenesis. *J. Exp. Zool.* **246**, 156–170 (1988).
34. B. Das, A. M. Schreiber, H. Huang, D. D. Brown, Multiple thyroid hormone-induced muscle growth and death programs during metamorphosis in *Xenopus laevis*. *Proc. Natl. Acad. Sci. U.S.A.* **99**, 12230–12235 (2002).
35. D. D. Brown, The role of thyroid hormone in zebrafish and axolotl development. *Proc. Natl. Acad. Sci. U.S.A.* **94**, 13011–13016 (1997).
36. E. M. Callery, R. P. Elinson, Thyroid hormone-dependent metamorphosis in a direct developing frog. *Proc. Natl. Acad. Sci. U.S.A.* **97**, 2615–2620 (2000).
37. N. Marsh-Armstrong, L. Cai, D. D. Brown, Thyroid hormone controls the development of connections between the spinal cord and limbs during *Xenopus laevis* metamorphosis. *Proc. Natl. Acad. Sci. U.S.A.* **101**, 165–170 (2004).
38. A. Nishikawa, H. Hayashi, Isoform transition of contractile proteins related to muscle remodeling with an axial gradient during metamorphosis in *Xenopus laevis*. *Dev. Biol.* **165**, 86–94 (1994).
39. C. Chanoine, S. Hardy, *Xenopus* muscle development: From primary to secondary myogenesis. *Dev. Dyn.* **226**, 12–23 (2003).
40. K. Shimizu-Nishikawa, Y. Shibota, A. Takei, M. Kuroda, A. Nishikawa, Regulation of specific developmental fates of larval- and adult-type muscles during metamorphosis of the frog *Xenopus*. *Dev. Biol.* **251**, 91–104 (2002).
41. W. E. Duellman, L. Trueb, *Biology of Amphibians* (The Johns Hopkins University Press, Baltimore, London, 1994).
42. A. Takisawa, Y. Sunaga, Uber die Entwicklung des M. depressor mandibulae bei Anuren im Laufe der Metamorphose [in German]. *Okajimas Folia Anat. Jpn.* **23**, 273–293 (1951).
43. K. E. Alley, Myofiber turnover is used to retrofit frog jaw muscles during metamorphosis. *Am. J. Anat.* **184**, 1–12 (1989).
44. H. J. de Jongh, *Functional morphology of the Jaw Apparatus of Larval and Metamorphosing Rana temporaria L* (Brill Archive, 1968).
45. J. Hanken, M. W. Klymkowsky, K. E. Alley, D. H. Jennings, Jaw muscle development as evidence for embryonic repatterning in direct-developing frogs. *Proc. Biol. Sci.* **264**, 1349–1354 (1997).
46. R. Altig, R. W. McDiarmid, Eds., *Tadpoles: The Biology of Anuran Larvae* (University of Chicago Press, Chicago, London, 1999).
47. K. Nishikawa, R. Wassersug, Morphology of the caudal spinal cord in *Rana* (Ranidae) and *Xenopus* (Pipidae) tadpoles. *J. Comp. Neurol.* **269**, 193–202 (1988).
48. K. Nishikawa, R. Wassersug, Evolution of spinal nerve number in anuran larvae. *Brain Behav. Evol.* **33**, 15–24 (1989).
49. W. Morse, Factors involved in the atrophy of the organs of the larval frog. *Biol. Bull.* **34**, 149–166 (1918).
50. H.-P. Gerber *et al*., VEGF couples hypertrophic cartilage remodeling, ossification and angiogenesis during endochondral bone formation. *Nat. Med.* **5**, 623–628 (1999).
51. L. Yang, K. Y. Tsang, H. C. Tang, D. Chan, K. S. E. Cheah, Hypertrophic chondrocytes can become osteoblasts and osteocytes in endochondral bone formation. *Proc. Natl. Acad. Sci. U.S.A.* **111**, 12097–12102 (2014).
52. M. Zenmyo *et al*., Morphological and biochemical evidence for apoptosis in the terminal hypertrophic chondrocytes of the growth plate. *J. Pathol.* **180**, 430–433 (1996).
53. Y. Ben-Ami *et al*., Transformation of fetal secondary cartilage into embryonic bone in organ cultures of human mandibular condyles. *Cell Tissue Res.* **271**, 317–322 (1993).
54. J. F. Durkin, Secondary cartilage: A misnomer? *Am. J. Orthod.* **62**, 15–41 (1972).
55. B. K. Hall, *Bones and Cartilage: Developmental and Evolutionary Skeletal Biology* (Elsevier, 2005).
56. A. Weiss, E. Livne, K. von der Mark, D. Heinegard, M. Silbermann, Growth and repair of cartilage: Organ culture system utilizing chondroprogenitor cells of condylar cartilage in newborn mice. *J. Bone Miner. Res.* **3**, 93–100 (1988).
57. W. A. Gosline, Functional morphology of the caudal skeleton in teleostean fishes. *Ichthyol. Res.* **44**, 137–141 (1997).
58. N. C. Bird, P. M. Mabee, Developmental morphology of the axial skeleton of the zebrafish, *Danio rerio* (Ostariophysi: Cyprinidae). *Dev. Dyn.* **228**, 337–357 (2003).
59. E. J. Hilton, G. D. Johnson, When two equals three: Developmental osteology and homology of the caudal skeleton in carangid fishes (Perciformes: Carangidae). *Evol. Dev.* **9**, 178–189 (2007).
60. A. Bensimon-Brito, M. L. Cancela, A. Huysseune, P. E. Witten, Vestiges, rudiments and fusion events: The zebrafish caudal fin endoskeleton in an evo-devo perspective. *Evol. Dev.* **14**, 116–127 (2012).
61. H.-P. Schultze, G. Arratia, Reevaluation of the caudal skeleton of some actinopterygian fishes: II. *Hiodon, Elops*, and *Albula*. *J. Morphol.* **195**, 257–303 (1988).
62. H.-P. Schultze, G. Arratia, The composition of the caudal skeleton of teleosts (Actinopterygii, Osteichthyes). *Zool. J. Linn. Soc.* **97**, 189–231 (1989).
63. F. Ferreri, C. Nicolais, C. Boglione, B. Bmertoline, Skeletal characterization of wild and reared zebrafish: Anomalies and meristic characters. *J. Fish Biol.* **56**, 1115–1128 (2000).
64. D. J. Rashid *et al*., From dinosaurs to birds: A tail of evolution. *Evodevo* **5**, 25 (2014).
65. D. J. Rashid *et al*., Avian tail ontogeny, pygostyle formation, and interpretation of juvenile Mesozoic specimens. *Sci. Rep.* **8**, 9014 (2018).
66. E. E. Maxwell, Ossification sequence of the avian order anseriformes, with comparison to other precocial birds. *J. Morphol.* **269**, 1095–1113 (2008).
67. M. M. Abitbol, Sacral curvature and supine posture. *Am. J. Phys. Anthropol.* **80**, 379–389 (1989).
68. C. R. Bardeen, Studies of the development of the human skeleton. (A). The development of the lumbar, sacral and coccygeal vertebrae. (B). The curves and the proportionate regional lengths of the spinal column during the first three months of embryonic development. (C). The development of the skeleton of the posterior limb. *Am. J. Anat.* **4**, 265–302 (1905).
69. J. A. Bar-Maor, K. M. Kesner, J. K. Kaftori, Human tails. *J. Bone Joint Surg. Br.* **62-B**, 508–510 (1980).
70. H. Holtzer, S. R. Detwiler, An experimental analysis of the development of the spinal column. III. Induction of skeletogenous cells. *J. Exp. Zool.* **123**, 335–369 (1953).

71. G. Strudel, L'influence morphogène du tube nerveux et de la corde sur la différenciation de la colonne vertébrale. *C. R. Seances Soc. Biol. Fil.* **147**, 132–133 (1953).
72. L. Ward, A. S. W. Pang, S. E. Evans, C. D. Stern, The role of the notochord in amniote vertebral column segmentation. *Dev. Biol.* **439**, 3–18 (2018).
73. G. Strudel, L'action morphogène du tube nerveux et de la corde sur la différenciation des vertèbres et des muscles vertébraux chez l'embryon de poulet. *Arch. Anat. Micr. Morph. Exp.* **44**, 209–235 (1955).
74. C. D. Stern, Mesoderm induction and development of the embryonic axis in amniotes. *Trends Genet.* **8**, 158–163 (1992).
75. D. J. Watterson, Problems in the evaluation of psychotherapy. *Bull. Menninger Clin.* **18**, 232–241 (1954).
76. R. L. Watterson, Development of the glycogen body of the chick spinal cord. III. The paired primordia as revealed by glycogen-specific stains. *Anat. Rec.* **113**, 29–51 (1952).
77. R. J. Wassersug, D. G. Sperry, The relationships of locomotion to differential predation on *Pseudacris triseriata* (Anura: Hylidae). *Ecology* **58**, 830–839 (1977).
78. R. B. Huey, Sprint velocity of tadpoles (*Bufo boreas*) through metamorphosis. *Copeia* **1980**, 537–540 (1980).
79. Y. Nakai, K. Nakajima, Y. Yaoita, Mechanisms of tail resorption during anuran metamorphosis. *Biomol. Concepts* **8**, 179–183 (2017).
80. Y. Yaoita, Tail resorption during metamorphosis in *Xenopus* tadpoles. *Front. Endocrinol. (Lausanne)* **10**, 143 (2019).
81. E. Ascarrunz, J.-C. Rage, P. Legreneur, M. Laurin, *Triadobatrachus massinoti*, the earliest known lissamphibian (Vertebrata: Tetrapoda) re-examined by μCT scan, and the evolution of trunk length in batrachians. *Contrib. Zool.* **85**, 201–234 (2016).
82. S. E. Evans, M. Borsuk-Białynicka, The early Triassic stem-frog *Czatkobatrachus* from Poland. *Palaeontologia Polonica* **65**, 79–105 (2009).
83. P. D. Nieuwkoop, J. Faber, *Normal Table of Xenopus laevis (Daudin)* (Garland Publishing Inc., New York, NY, 1994).
84. J. Hanken, R. Wassersug, The visible skeleton. *Funct. Photogr.* **16**, 22–26 (1981).
85. M. W. Klymkowsky, J. Hanken, Whole-mount staining of *Xenopus* and other vertebrates. *Methods Cell Biol.* **36**, 419–441 (1991).
86. L. Trueb, "Bones, frogs, and evolution" in *Evolutionary biology of the Anurans: Contemporary Research on Major Problems* (University of Missouri Press, Columbia, 1973), pp. 65–132.
87. L. Trueb, J. Hanken, Skeletal development in *Xenopus laevis* (Anura: Pipidae). *J. Morphol.* **214**, 1–41 (1992).
88. R. J. Denver, F. Hu, T. S. Scanlan, J. D. Furlow, Thyroid hormone receptor subtype specificity for hormone-dependent neurogenesis in *Xenopus laevis*. *Dev. Biol.* **326**, 155–168 (2009).
89. R. M. Harland, In situ hybridization: An improved whole-mount method for *Xenopus* embryos. *Methods Cell Biol.* **36**, 685–695 (1991).
90. P. O'Neill, R. B. McCole, C. V. H. Baker, A molecular analysis of neurogenic placode and cranial sensory ganglion development in the shark, *Scyliorhinus canicula*. *Dev. Biol.* **304**, 156–181 (2007).
91. G. Senevirathne *et al.*, Project: Ontogeny of the anuran urostyle and the developmental context of evolutionary novelty. MorphoSource. https://www.morphosource.org/Detail/ProjectDetail/Show/project_id/884. Deposited 3 December 2019.